JOURNAL OF MATERIALS SCIENCE 30 (1995) 3711–3719

Numerical solution to the solidification of aluminium in the presence of various fibres

M. A. KHAN, P. K. ROHATGI
University of Wisconsin-Milwaukee, Department of Materials Engineering, P.O. Box 784, Milwaukee, WI 53201, USA

In an attempt to understand the experimentally observed solidification microstructures in metal matrix composites, the influence of SiC, graphite and alumina fibres on the solidification of aluminium has been studied numerically. Irregular geometries of the composite material were mapped into simple rectangles through numerical conformal mapping techniques to analyse the influence of a single fibre or a row of fibres on a unidirectionally advancing planar solid–liquid interface. The fibres were assumed to be circular in cross-section and the direction of the interface movement was perpendicular to the length of the fibres. The study showed that for fibres with lower thermal conductivity than aluminium, the interface first goes through acceleration as it approaches and ascends the fibre and then deceleration as it descends the fibre. The acceleration and deceleration phenomena of the interface increases as the thermal conductivity ratio of fibre to liquid aluminium decreases. With low thermal conductivity ratios ($K_f/K_L \ll 1$), the interface is orthogonal to the fibre surface. When the conductivity of the fibre is lower than that of the melt, the interface becomes convex facing the fibre; this mode would lead to pushing of the fibre ahead if it was free to move, as has been experimentally observed in cast microstructures of metal matrix composites. The temperature versus solidification time plots of two points, one in the fibre and the other in aluminium, show that the fibre with a conductivity lower than the matrix is at a temperature higher than the melt; the temperature difference between the two points increases with increasing solidification rate for all the positions of the interface before it touches the fibre. The three-fibre study shows that as the number of fibres increases, the curvature of the interface increases upon approaching the subsequent fibres. The relationship between these numerical computations and experimental observations has been discussed.

Nomenclature

a reference length = diameter of the fibre

h Jacobian $= \left(\frac{\partial x}{\partial \xi}\right)^2 + \left(\frac{\partial y}{\partial \xi}\right)^2 = \left(\frac{\partial x}{\partial \eta}\right)^2 + \left(\frac{\partial y}{\partial \eta}\right)^2$

K thermal conductivity; in Equation 4 it is defined as $K'' = (K + K_f)/2$ for the common boundary between fibre and the freezing medium. For all the rest of the points $K'' = K$ in Equation 4

L latent heat of fusion

r non-dimensional variable in radial direction

S non-dimensional distance travelled by the interface

Ste Stefan number $= \frac{C_{ps}(T_m^* - T_0^*)}{L}$

T non-dimensional temperature

t non-dimensional time

x a non-dimensional spatial coordinate of physical plane

y a non-dimensional spatial coordinate of physical plane

α thermal diffusivity

η non-dimensional axial coordinate of the mapped plane

ξ non-dimensional vertical coordinate of the mapped plane

θ a polar coordinate

l liquid

m melting

s solid

O constant wall temperature

i initial

f fibre

* dimensional variables

1. Introduction

In recent years, considerable work has been done on the solidification of metal matrix composites containing either fibres or particulates as reinforcements. Solidification microstructure in metal matrix composites,

0022–2461

especially the uniformity in distribution of reinforcements, is important because it influences the physical and mechanical properties of these composites. Earlier experimental studies [1–4] on solidification of aluminium-, zinc- and magnesium-based composites containing fibres or particulates of graphite, alumina and silicon carbide, have shown that these reinforcements are generally segregated in the interdendritic regions when α phase is the primary solidifying phase (Fig. 1); similar microstructures have been reported by several workers in cast composites containing short fibres. This segregation presumably occurs due to the absence of nucleation of primary α phases on the reinforcements. In fact, α phases nucleate in the liquid between the reinforcements, and the change in the shape of the interface, during their growth push the particles or fibres, if they are free to move, into the interdendritic regions. The classical spherical cap theory of heterogeneous [5] nucleation indicates that nucleation should have preferentially occurred on the surfaces of reinforcements if their temperature was equal to or below the temperature of the liquid during cooling of the liquid–fibre mixture prior to the start of solidification. The fibre pushing, assuming it is free to move, is a result of various microforces arising due to thermal interaction of fibre with the liquid. Fluid mechanics (in general, Navier–Stokes equations) along with heat transfer (energy balance coupled with Navier–Stokes equations) teaches that these forces must be due to natural convection, pressure field, surface tension (when all three solid, liquid and fibre phases are in contact), and mass diffusion effects (for alloys only). In the case of alloys, the solidification takes place in a region called the mushy or two-phase zone; for pure substances, this region is extremely narrow and can be treated as a line or curve. This study, as a first step towards the complete solution of the fibre pushing problem, is directed at pure metals, motionless liquid and ignoring forces at the fibre–liquid boundary such as surface tension. The complete formulation of the unsteady state two-dimensional heat conduction problem on the mapped plane (see Fig. 4c) is given in Section 2. The details of the solution of the equations are given in Section 3. This study has great importance for two reasons; first, liquid metals are non-transparent and therefore the observation of the configuration of the solid–liquid front, as it approaches the fibre, is not possible; second, the various forces arising due to thermal interaction of fibre with liquid metal can only be determined by solving the relevant equations of heat transfer and fluid mechanics numerically, because experiments can only show fibre pushing but cannot determine forces pushing the fibre. In this paper, an attempt is made to calculate the rate of advancement of the solid–liquid interface, and the change in the shape of the interface, during unidirectional heat extraction from a liquid containing cylindrical fibres arranged in a square array. Also computed are the temperature differences between the fibres and the solidifying liquid during unidirectional solidification. These computations provide a framework for interrogating the thermal phenomenon and changes in the position and shape of the solidification front during unidirectional freezing of liquids in the presence of fibres both on a macroscopic scale and a microscopic scale.

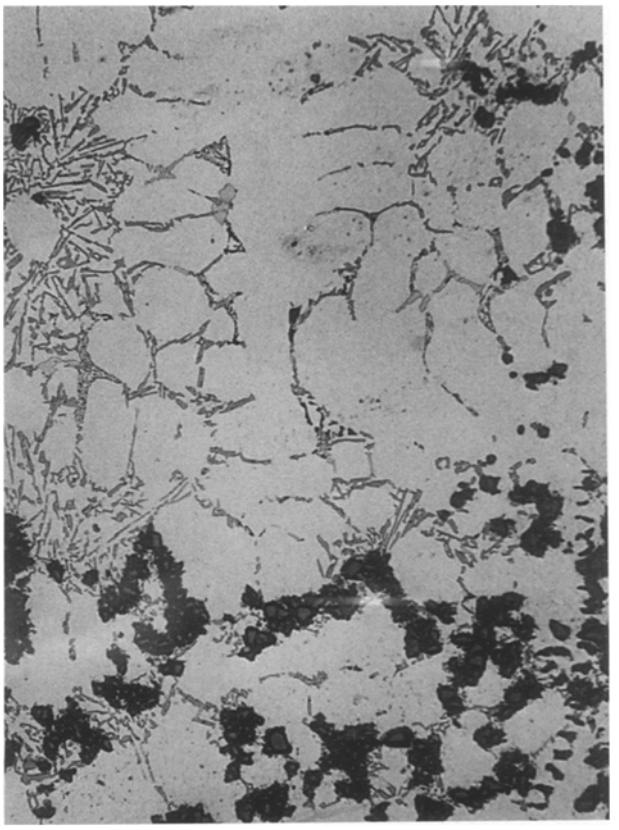

Figure 1 Microstructure of directionally solidified Al–10 vol % SiC composite, during a counter-gravity directional solidification experiment, showing lack of nucleation of α-aluminium on SiC particles; most of the SiC particles have been pushed into the interdendritic regions by α-aluminium dendrites.

The program used in this paper [6] solves for unidirectional solidification in the presence of a single fibre or an array of three fibres. Initially the program assumes uniform temperature in the melt and fibres. As an illustration a representative square array of fibres surrounded by the melt is schematically shown in Fig. 2.

The heat is extracted through the surface a–b such that surface a–b remains at constant temperature throughout the solidification process. The remaining surfaces of the mould are insulated. By symmetry the problem reduces to half as shown in Fig. 3. This configuration would simulate unidirectional solidification from constant-temperature chill in insulating moulds.

The solidification front, also referred to as an interface, starts at the surface a–b when the liquid metal at its initial temperature makes the first contact with this surface. Near the surface a–b, the advancing solidification front is flat without any curvature. As the front moves closer to the fibre, a curvature develops in the interface. The shape of this interfacial curvature depends on the thermal conductivity of the fibre relative to the thermal conductivity of the liquid. In the present study, the thermal conductivities of the various fibres used in the analysis were lower than the molten aluminium; these included fibres such as alumina. The

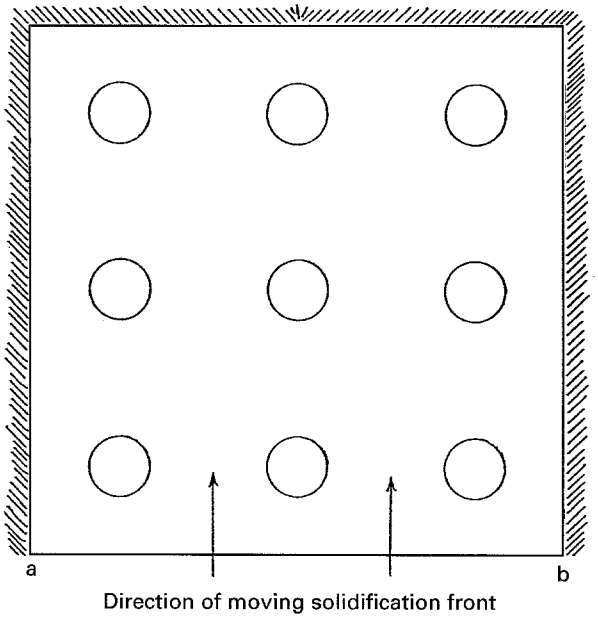

Figure 2 A set of circular non-metallic fibres in molten metal.

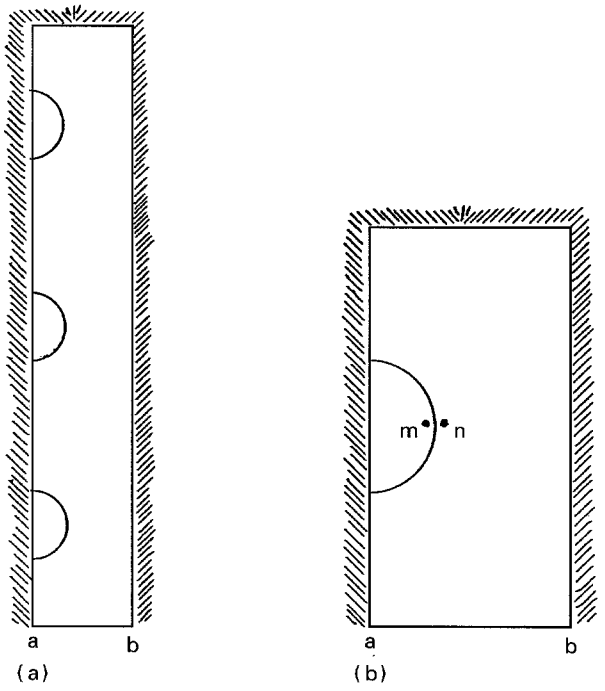

Figure 3 (a) The three-fibre problem. (b) The single fibre problem.

temperatures of points m and n (shown in Fig. 3b) were computed, together with the solidification time and the position of the interface.

The rate of advancement of the solidification front can be increased by lowering the temperature of the surface a–b (see Fig. 3) while keeping the temperature of the liquid and the fibres constant. Two different surface temperatures, T_0, were used to determine the influence of the interface speed on the temperature difference between points m and n. This would simulate the influence of increasing solidification rate by cooling the mould.

Three different fibres, SiC, alumina and graphite, were used in the analysis. The molten metal in all cases was pure aluminium. The problem was solved for cases with or without contact resistance between the fibre and aluminium (solid or liquid).

2. Problem formulation

The time method, initially developed by Khan and Landis [6], was used to obtain numerical results. Essentially, the time method uses an implicit finite difference scheme, which unlike the explicit scheme, is unconditionally stable for all time steps. It determines the time of solidification as the interface moves away from the cold surface. The position of the interface is fixed and known at one point, and this is where the time of solidification is determined.

It is difficult to match nodal points of cartesian and polar coordinates at the surface of the fibre (see Fig. 3). Also, to satisfy the orthogonal heat flux boundary condition at the surface of the fibre, it would introduce additional error because cartesian coordinates are non-orthogonal to the surface of the fibre. It was decided, therefore, to generate curvilinear coordinates for the rather complicated geometry of Fig. 3. Coformal mapping produces the best coordinates in that the grid is orthogonal, has the simplest transformation Jacobian and the transformed equations on the mapped plane are the least complicated.

The solidification problem was solved on the mapped plane (see Fig. 4c). Numerical conformal mapping techniques, similar to Ives and Zacharias [7], were used to generate curvilinear coordinates for a single and three fibres shown in Fig. 4a and b. Points of the physical contour were so picked that the grid obtained on the mapped plane was equi-spaced. For the purpose of reducing error, in starting the solution of the solidification problem, two coordinates were placed very close to the isothermal surface a–b in Fig. 4a and b. The non-dimensional solution of a conduction heat-transfer problem on non-dimensional geometries of Fig. 4a and b is independent of the size of the fibres as long as the ratio of fibre diameter (one unit in Fig. 4a) to the cell geometry (1.5 units × 3 units) is kept constant. For example, if the fibre diameter is 10 μm, then the cell geometry would be 15 μm × 30 μm.

Initially a mould with one or three fibres (see Fig. 2) was at a uniform temperature, T_i. The fibres were in thermal equilibrium with molten metal surrounding them. At some time $t > 0$, the lower surface a–b (see Fig. 3) was subjected to a constant temperature, T_0, much lower than the melting point temperature of the metal. Solidification started and there existed solid and liquid phases, separated by a surface to be called an interface which is assumed to be planar. All the properties of liquid, solid and fibre phases were assumed to be constant; these values are given in Table I. The problem was solved with and without contact resistance which might be present between the fibre and aluminium (solid or liquid phase).

The main assumptions made in this study are that the liquid is still (without motion) during the entire solidification process and there are no forces involved at the fibre–liquid boundary. Thus it is a transient conduction heat transfer problem on the mapped plane (Fig. 4c); where temperature in the solid, liquid

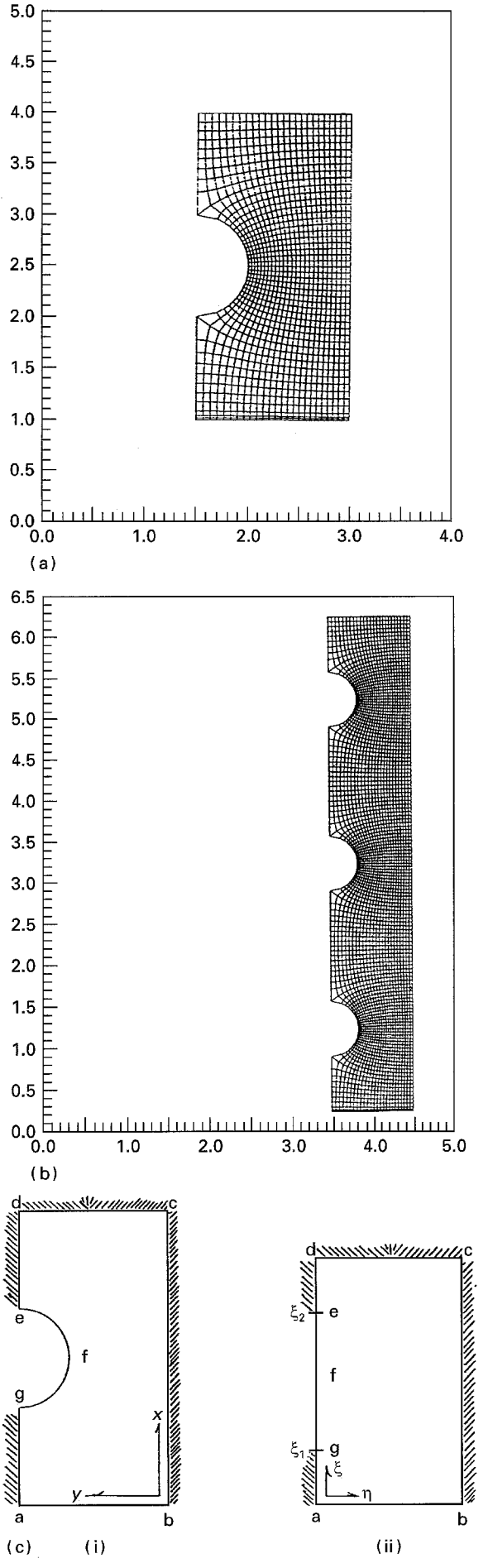

Figure 4 (a) Curvilinear coordinates of a single fibre (equi-spaced grid points = 26 × 46). (b) Curvilinear coordinates of three fibres inter-fibre spacing = 2 diameters (c) (i) Physical plane and (ii) mapped plane of a single fibre.

TABLE I Thermal properties of aluminium and fibres (graphite, alumina and silicon carbide) used in this study

Properties	Aluminium	Graphite	Alumina	Silicon carbide
K_s (W m^{-1} K^{-1})	237.65	23.85	3.975	12.97
K_L (W m^{-1} K^{-1})	94.14	–	–	–
ρ (kg m^{-3})	2700.00	2250.00	3970.0	3200.00
C_{p_s} (J kg^{-1} °C^{-1})	903.74	690.36	1071.1	841.00
C_{p_L} (J kg^{-1} °C^{-1})	1079.47	–	–	–
L (J kg^{-1})	397480.00	–	–	–
T_m (°C)	660.00	–	–	–

and fibre phases is determined at each nodal point as a function of time during the solidification process. The latent heat along with the sensible heat is included in the energy balance at the solid–liquid front.

The following variables were used to non-dimensionalize the problem.

$$T = \frac{T^* - T_m^*}{T_m^* - T_0^*} \tag{1a}$$

$$\xi = \frac{\xi^*}{a} \tag{1b}$$

$$\eta = \frac{\eta^*}{a} \tag{1c}$$

$$r = \frac{r^*}{a} \tag{1d}$$

$$S = \frac{S^*}{a} \tag{1e}$$

$$t = \frac{\alpha_s t^*}{a^2} \tag{1f}$$

The Fourier number, t, was non-dimensionalized with α_s or α_f, whichever was the largest. It is further discussed in Section 4. The non-dimensional equations of the mapped plane then become (see Fig. 4c)

$$\frac{\partial^2 T_s}{\partial \xi^2} + \frac{\partial^2 T_s}{\partial \eta^2} = h\frac{\partial T_s}{\partial t} \tag{2a}$$

$$T_s = -1 \quad \text{at } \xi = 0; \quad 0 \leqslant \eta \leqslant \eta_0; \quad t > 0 \tag{2b}$$

$$\frac{\partial T_s}{\partial \eta} = 0 \quad \text{at } \eta = \eta_0; \quad 0 \leqslant \xi \leqslant \xi_0; \quad t > 0 \tag{2c}$$

$$\frac{\partial T_s}{\partial \eta} = 0 \quad \text{at } \eta = 0; \quad \xi_2 \leqslant \xi \leqslant \xi_1; \quad t > 0 \tag{2d}$$

$$\frac{\partial^2 T_L}{\partial \xi^2} + \frac{\partial^2 T_L}{\partial \eta^2} = h\frac{\alpha_s}{\alpha_L}\frac{\partial T_L}{\partial t} \tag{3a}$$

$$T_L = T_i \quad \text{at } t = 0; \quad \xi, \eta \geqslant 0 \tag{3b}$$

$$\frac{\partial T_L}{\partial \xi} = 0 \quad \text{at } \xi = \xi_0; \quad 0 \leqslant \eta \leqslant \eta_0; \quad t > 0 \tag{3c}$$

$$\frac{\partial T_L}{\partial \eta} = 0 \quad \text{at } \eta = \eta_0; \quad 0 \leqslant \xi \leqslant \xi_0; \quad t > 0 \tag{3d}$$

$$\frac{\partial T_L}{\partial \eta} = 0 \quad \text{at } \eta = 0; \quad \xi_2 \leqslant \xi \leqslant \xi_1; \quad t > 0 \tag{3e}$$

$$T_L = T_s = T_m = 0 \quad \text{at } \xi = S(\eta, t); \quad t > 0 \tag{3f}$$

$$\left[1 + \left(\frac{\partial s}{\partial \eta}\right)^2\right]\left[\frac{\partial T_s}{\partial \xi} - \frac{K_L''}{K_s''}\frac{\partial T_L}{\partial \xi}\right] = \frac{hK_s}{K_s''\,\mathrm{Ste}}\frac{\partial s}{\partial t}$$

$$\text{at } \xi = S(\eta, t); \quad t > 0 \tag{4}$$

$$\frac{\partial^2 T_f}{\partial r^2} + \frac{1}{r}\frac{\partial T_f}{\partial r} + \frac{1}{r^2}\frac{\partial^2 T_f}{\partial \theta^2} = \frac{\alpha_s}{\alpha_f}\frac{\partial T_f}{\partial t}; \quad t > 0 \tag{5a}$$

$$\frac{\partial T_f}{\partial \theta} = 0 \quad \text{at } \theta = 0; \quad 0 \leqslant r \leqslant 0.5; \quad t > 0 \tag{5b}$$

$$\frac{\partial T_f}{\partial \theta} = 0 \quad \text{at } \theta = \pi; \quad 0 \leqslant r \leqslant 0.5; \quad t > 0 \tag{5c}$$

$$\frac{\partial T_f}{\partial r} = 0 \quad \text{at } r = 0; \quad t > 0 \tag{5d}$$

Without contact resistance

$$T_f = T_j \quad \text{at } r = 0.5; \quad 0 \leqslant \theta \leqslant \pi; \quad t > 0 \tag{6a}$$

With contact resistance

$$T_j - T_f = R_C'' K_f \frac{\partial T_f}{\partial r}$$

$$\text{at } r = 0.5; \quad 0 \leqslant \theta \leqslant \pi; \quad t > 0 \tag{6b}$$

$$\frac{\partial T_f}{\partial r} = \frac{K_j}{K_f}\frac{1}{h^{1/2}}\frac{\partial T_j}{\partial \eta} \quad \begin{matrix} r = 0.5 \\ \text{at } 0 < \theta < \pi \\ t > 0 \end{matrix} \tag{6c}$$

where $j \equiv L$ or S.

3. Solution of the equations on the mapped plane

Equations 2 and 3 are two-dimensional unsteady state conduction heat transfer equations of the solid and liquid phases, respectively. The relevant boundary conditions indicate (see Fig. 4c) that the lower boundary a–b was subjected to a constant temperature, T_0, much lower than melting point temperature, T_m; and the surfaces b–c, c–d, d–e and g–a were insulated. The initial condition is given in Equation 3b. The matching condition between the liquid and solid phases is Equation 3f. The energy balance at the solid–liquid interface that includes the Ste (the Stefan number, which includes latent heat) is given in Equation 4. The temperature distribution in the fibre was determined by using polar coordinates in the physical plane (Equation 5a); the details of the physical plane including fibres are given in Fig. 3. The matching conditions between fibre and metal are given in Equations 5d, 6b and 6c. The contact resistance arises due to the presence of gas which creates additional resistance to heat flow through the surface of the fibre. The presence of gas around fibres may be either due to poor wettability of the fibres or due to the degassing process of some liquid metals. Equation 6b and c is the orthogonal heat flux balance between the fibre and surrounding metal.

Equations 2–6 were solved using a finite difference scheme on a mesh which was equi-spaced in both ξ and η directions except that two additional grid lines were added in the ξ direction at the cold surface, a–b, of Fig. 2 to allow for starting the solution. In the single fibre case, the number of equi-spaced grid points were 46 in the ξ direction and 26 in the η direction. The non-dimensional temperatures were converged to 10^{-4} and the time step to 10^{-5}. The iterative solution was converged by combining a Newton method with successive over-relaxation (SOR) scheme. The interface was located with the time method described elsewhere [6]. Because Equation 5a cannot be solved at $r = 0$, an alternative form derived from L'Hospital's rule can be used

$$2\frac{\partial^2 T_f}{\partial y^2} = \frac{\alpha_s}{\alpha_f}\frac{\partial T_f}{\partial t} \tag{7}$$

There are also other ways to get around this difficulty at $r = 0$. The equation that was used in the present work is as follows

$$\frac{\partial^2 T_f}{\partial x^2} + \frac{\partial^2 T_f}{\partial y^2} = \frac{\alpha_s}{\alpha_f}\frac{\partial T_f}{\partial t} \tag{8}$$

where x and y would represent cartesian coordinates at $r = 0$.

4. Results and discussion

The solidification of aluminium in the presence of fibres was studied with respect to changes in (a) the initial temperature of the melt, (b) the cold surface temperature of the melt, and (c) the properties of the fibre. The study was conducted with and without contact resistance at the fibre and aluminium interface.

The positions and shapes of the solidification front at successive time intervals plotted for graphite and alumina are shown in Fig. 5a–c. The plots are shifted by 0.5 in ($\sim$1.25 cm) from the origin for the purpose of clarity. Three different fibres (SiC, Al_2O_3 and graphite) were used in the solidification of aluminium. The effect of interfacial resistance at the fibre–metal interface on the positions and shape of the solidification front at successive time intervals was studied. The values of interface resistance chosen are typical values obtained across metal–mould interfaces. In all of the plots (Fig. 5a–c), there is an acceleration of the interface as it approaches and ascends the fibre, and deceleration as it descends the fibre. The acceleration and deceleration basically depend on the thermal conductivity ratio of the fibre to the melt. As this ratio decreases from graphite to Al_2O_3 (Fig. 5b compared with 5a), there is more acceleration and deceleration phenomena of the interface near the fibre. To compare these plots one can check the position of the last interface near the fibre and the differences become obvious. When the mould surface temperature was varied from 460–260 °C while keeping the initial temperature of the melt (720 °C) constant, there was no

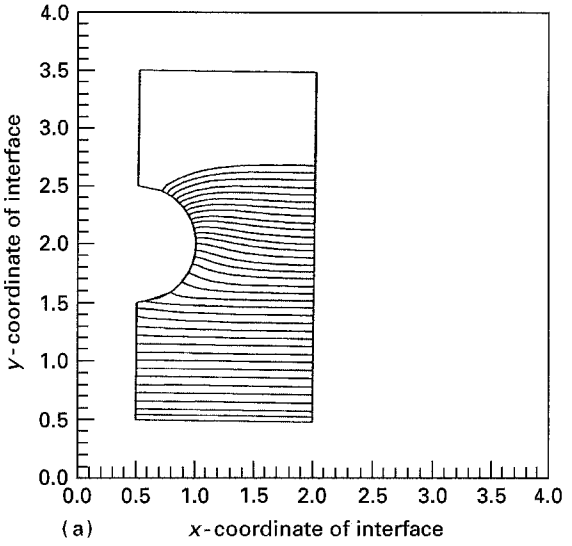

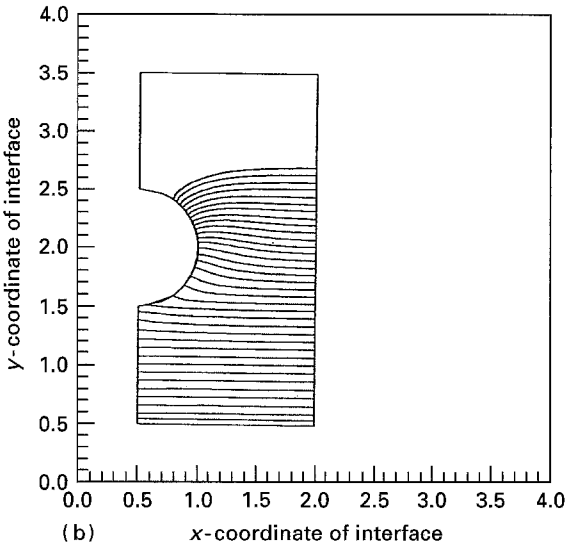

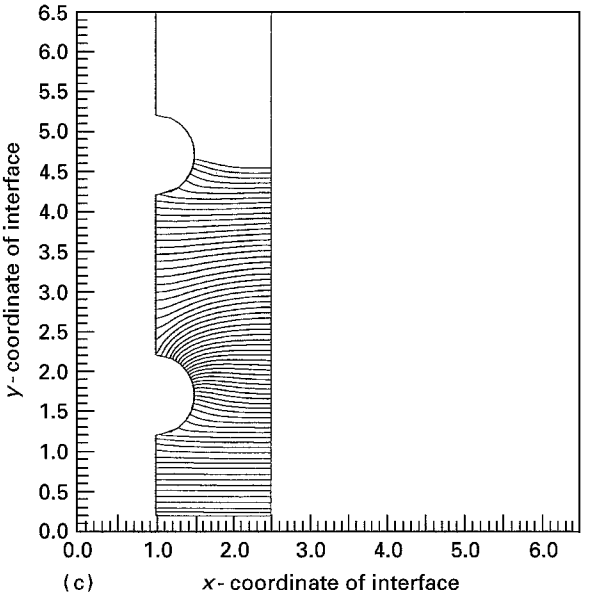

Figure 5 (a) Configuration of the solidification front of aluminium during interaction with graphite fibre. Mould wall temperature = 460 °C; initial melt–fibre temperature = 720 °C; no metal–fibre interface resistance. (b) Configuration of the solidification front of aluminium during interaction with alumina fibre. Mould wall temperature = 460 °C; initial melt–fibre temperature = 720 °C; no metal–fibre interface resistance. (c) Configuration of the solidification front of aluminium during interaction with three alumina fibres. Mould wall temperature = 460 °C; initial melt–fibre temperature = 720 °C; no metal–fibre interface resistance.

apparent variation in the shape of the interface except for the increase in the rate of advancement of the solidification front. The region of acceleration of the interface can be interpreted as a region of low heat flux. The interface appears to be more orthogonal to the fibre as the thermal conductivity ratio of the fibre to the melt decreases. Because the heat flux lines are always orthogonal to the isotherms (solid–liquid interface) for the case of the conduction problem, it can therefore be concluded that as the thermal conductivity of the fibre becomes very low compared to the melt, the surface of the fibre is always a line of the heat flux. The curvature in the interface as it approaches the fibres is important in influencing whether the fibres will have a tendency to be entrapped by a concave outward interface or pushed ahead by a convex outward interface.

Fig. 5c shows the positions of the solidification front for the three alumina fibres case. For purpose of brevity only two fibres are shown. The three-fibre study shows that as the interface passes the first fibre, it goes through acceleration until and up to the time it ascends to the second fibre. The curvature of the interface is more, as it arrives at the second fibre compared to the same position of the interface near the first fibre. This plot shows the effects of more than one fibre in the melt on the shape of the solid–liquid interface. Clearly as the number of successive fibres increases, the curvature of the interface increases as it approaches the individual fibres. This will have commensurate influence on the particle pushing phenomenon, which would appear to become easier, in the presence of a long array of fibres.

The program [6] was modified to incorporate the interfacial resistance between the fibre and aluminium, and cases such as alumina and graphite with and without any resistance at the melt–fibre interface were studied. The influence of fibre–metal resistance of $10^{-4}\,m^2\,K\,W^{-1}$ on the alumina fibre is negligible because alumina itself has a very small thermal conductivity; therefore an additional small resistance would cause a relatively small change in the shape of the interface. As the fibre–metal contact resistance was increased from 10^{-4} to $10^{-3}\,m^2\,K\,W^{-1}$ for graphite, the acceleration and deceleration of the interface increased. The increase in contact resistance is equivalent to lowering the thermal conductivity of the fibre. The contact resistance effects will be further discussed with regard to temperature differences between the fibres and aluminium. The influence of initial temperature of molten aluminium on the positions and shapes of solidification fronts was studied; there are no significant changes except for the time delay in the position of solidification front on arrival of the interface at a particular position.

The temperature of points m (in the fibre) and n (in the aluminium) shown in Fig. 3b are plotted in Fig. 6a–g as a function of solidification time. These temperature differences are important because they

influence whether nucleation of primarily α can occur on the fibre ahead of the macroscopic solidification front. For instance, if the fibre is hotter than the melt, nucleation is not possible. If the fibre is substantially cooler, nucleation may occur. In Fig. 6a, at the initial melt fibre temperature of 720 °C, the maximum temperature difference is 45 °C between alumina fibre and aluminium at a solidification time of 27.5 s. When a contact resistance of 10^{-4} $m^2 K W^{-1}$ was placed on the same fibre with the same initial and wall temperatures, the maximum temperature difference of 50 °C occurred after 30 s solidification time. The time delay and increase in temperature differences are due to the effects of contact resistance. In Fig. 6b, the mould wall temperature was decreased to 260 °C while the initial temperature was kept the same, the maximum temperature difference of 90 °C occurred at a solidification time of 21.9 s. This shows that with faster solidification rate, the maximum temperature difference between alumina fibre and aluminium significantly increases. For the same fibre, with a high initial melt temperature of 760 °C for a wall temperature of 460 °C, the maximum temperature difference between fibre and aluminium was found to be 60 °C at a solidification time of 25 s. Three alumina fibres placed in consecutive order were also studied (see Fig. 5e). In the case of three alumina fibres (Fig. 6d), the maximum temperature difference of 45.5 °C occurred at a solidification time of 27 s. The temperature difference was recorded for the first fibre only. This appears to be in close agreement with temperature difference of Fig. 6a. Thus multiple fibre effects on the first fibre are not significant in regard to temperature differences, because alumina has a very low thermal conductivity compared to aluminium and therefore the alumina fibre always acts as a heat source.

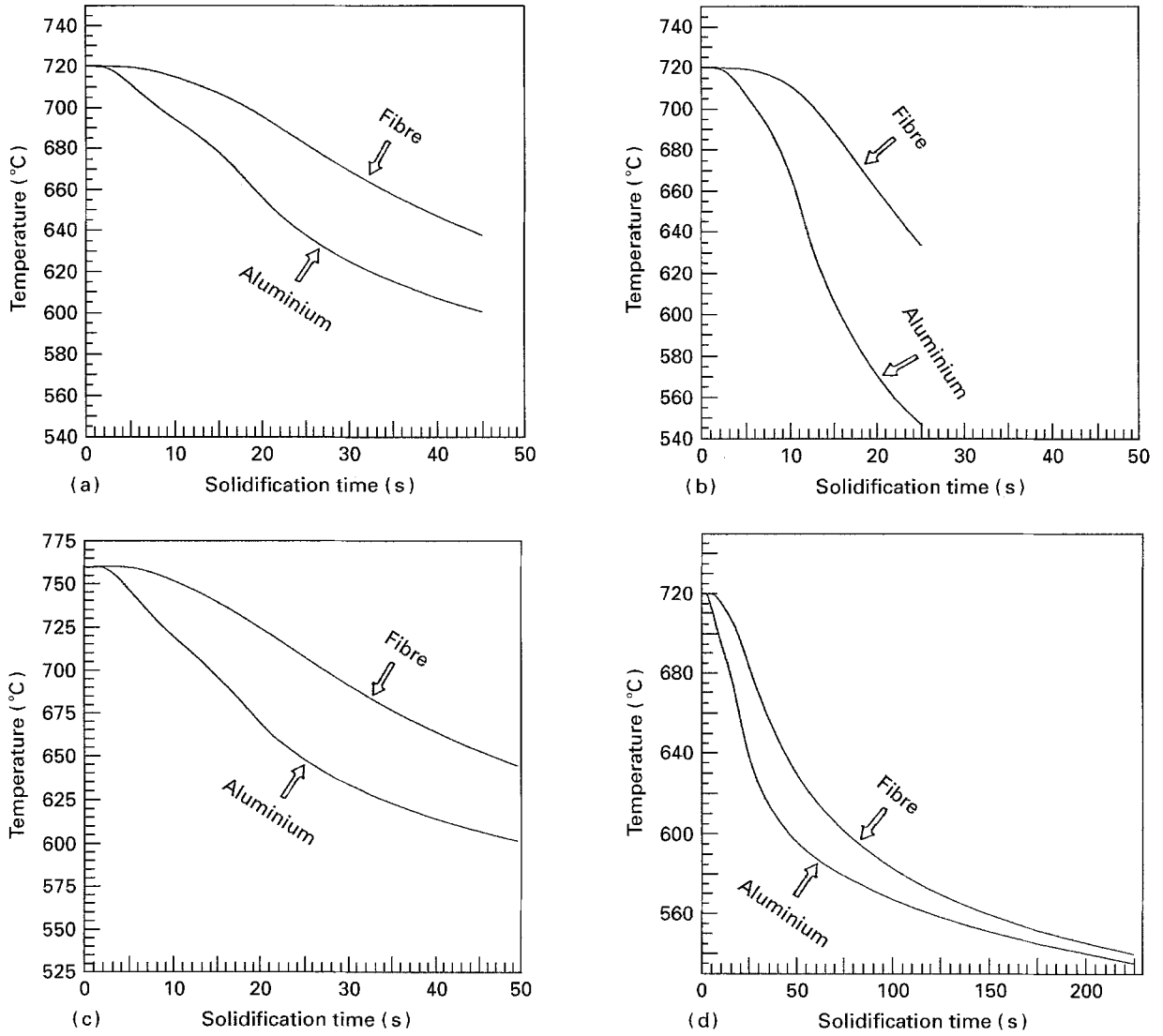

Figure 6 (a) Temperatures of points m and n (Fig. 3b) of a single alumina fibre. Mould wall temperature = 460 °C; initial melt–fibre temperature = 720 °C; no metal–fibre interface resistance. (b) Temperatures of points m and n (Fig. 3b) of a single alumina fibre. Mould wall temperature = 460 °C; initial melt–fibre temperature = 720 °C; no metal–fibre interface resistance. (c) Temperatures of points m and n (Fig. 3b) of a single alumina fibre. Mould wall temperature = 460 °C; initial melt–fibre temperature = 760 °C; no metal–fibre interface resistance. (d) Temperatures of points m and n (Fig. 3a) of three-alumina fibres. Mould wall temperature = 460 °C; initial melt–fibre temperature = 720 °C; no metal–fibre interface resistance. (e) Temperatures of points m and n (Fig. 3b) of a single SiC fibre. Mould wall temperature = 460 °C; initial melt–fibre temperature = 720 °C; no metal–fibre interface resistance. (f) Temperatures of points m and n (Fig. 3b) of a single graphite fibre. Mould wall temperature = 460 °C; initial melt–fibre temperature = 720 °C; no metal–fibre interface resistance. (g) Temperatures of points m and n (Fig. 3b) of a single graphite fibre. Mould wall temperature = 460 °C; initial melt–fibre temperature = 720 °C; metal–fibre interface resistance = 10^{-3} $m^2 K W^{-1}$.

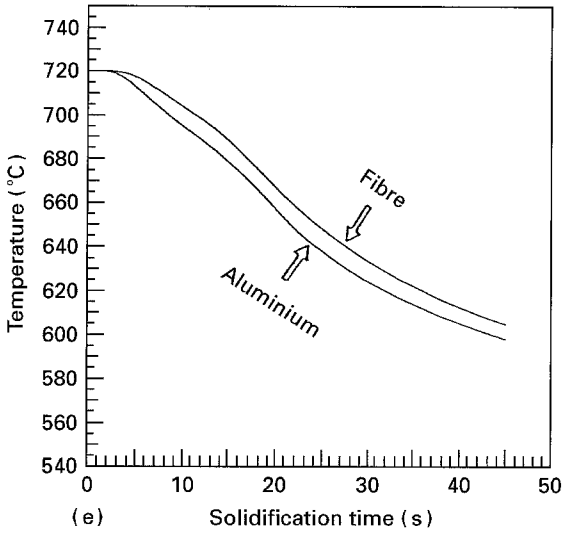

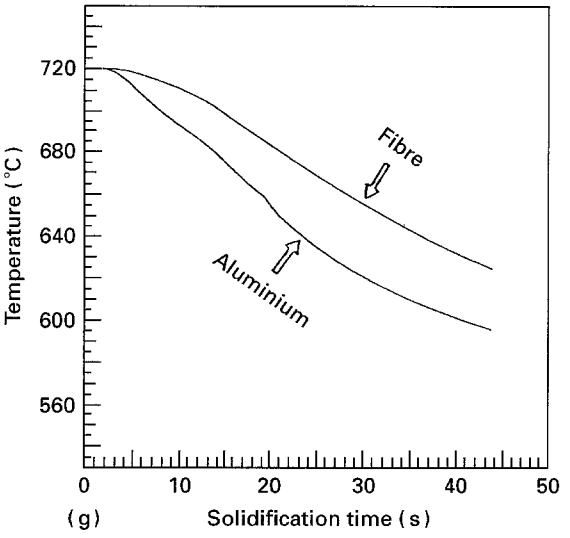

The Al–SiC study (Fig. 6e) shows a maximum temperature difference of 10 °C at a solidification time of 22.5 s. As the initial mould wall temperature was lowered to 260 °C, the maximum temperature difference of 27.6 °C occurred at 15 s solidification time. Once again, as in the case of alumina fibre, there is a significant temperature difference between the fibre and aluminium as the wall temperature is decreased.

The aluminium–graphite study (see Fig. 6f) was peculiar in that first the fibre temperature up to a solidification time of 15 s was higher than the aluminium, then from 15–21 s solidification time, the fibre temperature was lower than the aluminium. From 21–44.5 s the fibre temperature was again higher than the aluminium. When a contact resistance of $10^{-4}\,m^2KW^{-1}$ was placed on the fibre, the maximum temperature difference of 5.8 °C occurred at 10.7 s. As in the case of Al_2O_3 and SiC fibres, the temperature of the graphite always remained above that of the aluminium. A further increase in contact resistance to $10^{-3}\,m^2KW^{-1}$, shown in Fig. 6g, has a significant effect on the temperature difference (34 °C at 32.6 s). Thus, in the case of the aluminium–graphite system, the fibre temperature always remains above the aluminium if a contact resistance of $10^{-4}\,m^2KW^{-1}$ or more is imposed on the fibre. When the wall temperature was dropped to 260 °C, the results without contact resistance show

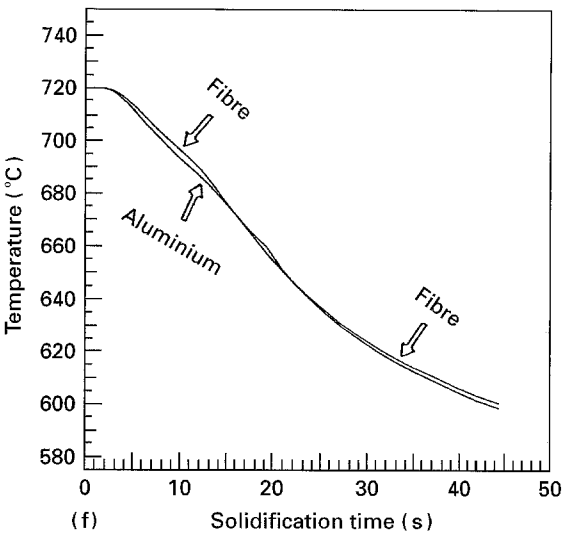

Figure 6 Continued.

that the fibre is at a higher temperature up to 8.8 s, and then drops to a lower temperature than aluminium up to 11 s solidification time. From 11–24.6 s, the fibre is once again at a higher temperature than the aluminium. The maximum temperature difference of 6.6 °C occurred at 20.5 s solidification time. The case of aluminium–graphite fibres clearly demonstrates the possibility of altering the temperature differences between the fibres and the melt by changing mould conditions.

The distance of the solid–liquid interface versus solidification time has been computed for each case discussed above, and a typical plot showing the influence of mould temperature and the initial melt–fibre temperature is shown in the Appendix (Fig. A1). These curves show typical parabolic shapes qualitatively validating the computations; in addition they illustrate the influences of the fibre, changes in initial melt–fibre and mould wall temperatures on the rate of advancement of the solidification front.

5. Conclusions

A numerically computed rate of advancement of the solidification front of a liquid from a constant temperature chill surface in the presence of fibres in the melt has been presented. The method also permits computations of shapes of the solidification front and the differences in temperatures between the fibres and the melt during solidification. As the ratio of the thermal conductivity of the fibre to that of aluminium decreases, the acceleration of the planar solidification interface, while approaching and ascending the fibre, increases. This behaviour can be attributed to the presence of a low heat flux coming through the fibre in that region, compared to the situation when no fibre is present. The greatest acceleration of the interface occurs as it is ascending roughly the first quarter of the fibre. Thereafter, deceleration of the interface starts, implying that heat flux is increasing. The deceleration becomes more obvious as the interface descends the fibre. The effect of a contact resistance across the metal–fibre interface, on the motion of the interface is

equivalent to lowering the thermal conductivity of the fibre.

For lower thermal conductivity ratios of the fibre to aluminium, the solid–liquid interface (an isotherm) is always orthogonal to the surface of the fibre irrespective of acceleration or deceleration of the interface there. This means that, for $K_f/K_L \ll 1$, the surface of the fibre is a varying heat flux surface for the case of the conduction heat-transfer problem.

The temperature plots show that as the thermal conductivity ratio of fibre to aluminium decreases, the temperature difference between fibre and aluminium becomes significant; the temperature of molten aluminium is lower than the fibre. As the temperature difference between the melting point temperature and the mould wall temperature is decreased by a factor of two, the maximum temperature difference between fibre and aluminium increases by a factor of two or more. In other words, the faster cooling rates decrease the maximum temperature difference between fibre and aluminium, thereby decreasing the barrier to nucleation on the fibres. The effect of contact resistance between the metal and the fibre is to increase further the temperature difference between the fibre and aluminium.

The results indicate that when the thermal conductivity of the fibres is lower than that of the melt, the fibres are at a temperature higher than the melt for most of the cases investigated in this study; this is perhaps one of the reasons why nucleation of primary α phases on the particles is generally not observed during solidification of composites such as aluminium–alumina, aluminium–graphite and aluminium–silicon carbide. The method presented in this paper permits interrogation of temperature differences and solidification front patterns for different composites under different freezing conditions. This framework can help in process design to alter microstructures formed on solidification of metal matrix composites.

Appendix

Fig. A1 shows the plot of interface distance versus the solidification time. The distance travelled by the interface over line b–c in Fig. 4c(i), was recorded for each solidification time that the interface takes to arrive at a given position. The slope of these curves is the speed of the interface. For the plot where the solidification time is short, i.e. the wall temperature is low, the slope of the curve is very steep. The speed of the interface is related to temperature gradients (see Equation 4) in solid and liquid phases. The slope of the interface at line b–c of Fig. 4c(i) is zero, thus the speed of the interface is entirely determined by the difference of temperature gradients in solid and liquid phases over line b–c. Temperature gradients as well as the speed of the interface are important in understanding the formation of solidification microstructures. Fig. A1

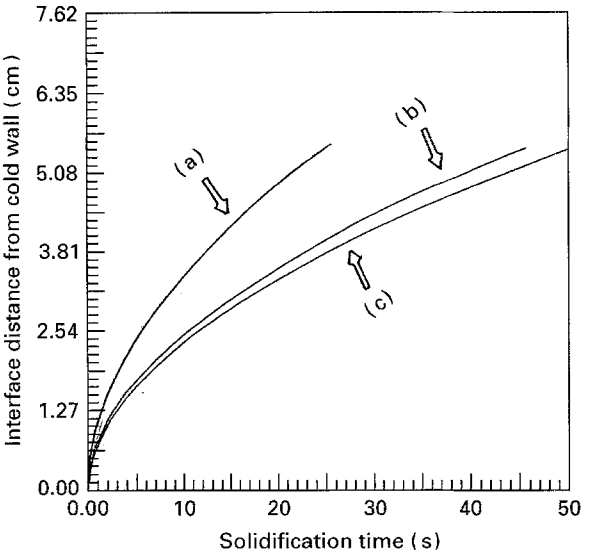

Figure A1 Interface distance versus time over the line of symmetry of a single alumina fibre. Mould wall temperature = 460 °C; initial melt–fibre temperature = 720 °C; no metal–fibre interface resistance.

clearly shows the effect of superheat as the initial melt–fibre temperature is increased from 720 °C to 760 °C. Also the mould wall temperature was varied from 460–260 °C shown as curve(a) in Fig. A1.

References

1. P. K. ROHATGI, R. ASTHANA and S. DAS, *Int. Mater. Rev.* **31** (1986) 115.
2. P. K. ROHATGI, R. ASTHANA and F. YARANDI, in "Solidification of metal-matrix composites", edited by P. K. Rohatgi (TMS/AIME, Warrendale, PA, 1990) p. 5.
3. B. C. PAI, S. RAY, K. V. PRABHAKAR and P. K. ROHATGI, *Mater. Sci. Eng.* **24**(1) (1976) 31.
4. P. K. ROHATGI and M. K. SURAPPA, *ibid.* **62**(2) (1984) 159.
5. S. RAY, M. S. BHAT and P. K. ROHATGI, *Scripta Metall. Mater.* (1991) submitted.
6. M. A. KHAN, PhD thesis, University of Wisconsin-Milwaukee (1990).
7. D. C. IVES and R. M. ZACHARIAS, Conformal mapping and orthogonal grid generation, AIAA/SAE/AMSE/ASEE 23rd Joint Propulsion Conference, 29 June–2 July, San Diego, CA (1987).
8. M. N. OZISIK, "Heat conduction" (Wiley, New York, 1980).
9. N. B. VERGAFTIK, "Tables on the thermophysical properties of liquid and gases" (Wiley, New York, 1975).
10. R. W. GALLANT, "Physical properties of hydrocarbons" (Gulf, Houston, TX, 1968).
11. K. RAZNJEVIC, "Handbook of thermodynamic tables and charts" (Hemisphere, Washington, 1976).
12. R. R. DREISBACH, "Physical Properties of Chemical Compounds" (American Chemical Society, 1955).
13. T. IIDA and R. I. L. GUTHRIE, "The physical properties of liquid metals" (Clarendon Press, Oxford, 1988).
14. J. F. THOMPSON, Z. U. A. WARSI and C. W. MASTIN, "Numerical grid generation: Foundations and applications (North-Holland, Elsevier, 1985).

Received 9 September 1993
and accepted 21 March 1994